AD-A194 994 ANALYSIS OF ENVIRONMENTAL PARAMETERS FROM THE PANAMA CITY TOWER RADAR EXPERIMENT(U) NAVAL RESEARCH LAB WASHINGTON DC L U MARTIN ET AL 12 APR 88 NRL-MR-6100 1/1

UNCLASSIFIED F/G 17/9 NL

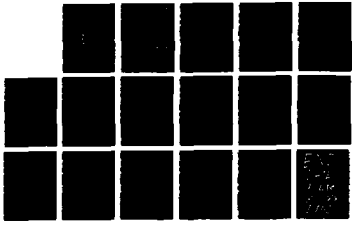

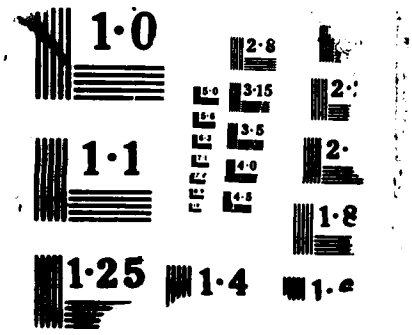
1·0
1·1
1·25
1·4
2·8
3·15
3·5
4·0
4·5
1·8

Naval Research Laboratory
Washington, DC 20375-5000

NRL Memorandum Report 6100

Analysis of Environmental Parameters from the Panama City Tower Radar Experiment

LEE U. MARTIN AND DENNIS B. TRIZNA

Radar Propagation Staff
Radar Division

April 12, 1988

SECURITY CLASSIFICATION OF THIS PAGE

ADA194994

REPORT DOCUMENTATION PAGE

Form Approved
OMB No. 0704-0188

1a. REPORT SECURITY CLASSIFICATION UNCLASSIFIED	1b. RESTRICTIVE MARKINGS
2a. SECURITY CLASSIFICATION AUTHORITY	3. DISTRIBUTION/AVAILABILITY OF REPORT Approved for public release; distribution unlimited.
2b. DECLASSIFICATION/DOWNGRADING SCHEDULE	
4. PERFORMING ORGANIZATION REPORT NUMBER(S) NRL Memorandum Report 6100	5. MONITORING ORGANIZATION REPORT NUMBER(S)
6a. NAME OF PERFORMING ORGANIZATION NRL Research Laboratory 6b. OFFICE SYMBOL (If applicable) NRL (5303)	7a. NAME OF MONITORING ORGANIZATION Office of Naval Research
6c. ADDRESS (City, State, and ZIP Code) Washington, D.C. 20375-5000	7b. ADDRESS (City, State, and ZIP Code) Arlington, VA 22217
8a. NAME OF FUNDING/SPONSORING ORGANIZATION Office of Naval Research 8b. OFFICE SYMBOL (If applicable) ONR	9. PROCUREMENT INSTRUMENT IDENTIFICATION NUMBER
8c. ADDRESS (City, State, and ZIP Code) Arlington, VA 22217	10. SOURCE OF FUNDING NUMBERS PROGRAM ELEMENT NO. 61153N; PROJECT NO. RR021-05-43; TASK NO.; WORK UNIT ACCESSION NO. DN 280-045

11. TITLE (Include Security Classification)
Analysis of Environmental Parameters from the Panama City Tower Radar Experiment

12. PERSONAL AUTHOR(S)
Martin, Lee U., and Trizna, Dennis B.

13a. TYPE OF REPORT	13b. TIME COVERED	14. DATE OF REPORT (Year, Month, Day)	15. PAGE COUNT
Interim	FROM Jan 86 TO Jun 87	1988 April 12	32

16. SUPPLEMENTARY NOTATION

17. COSATI CODES		
FIELD	GROUP	SUB-GROUP

18. SUBJECT TERMS (Continue on reverse if necessary and identify by block number)
Radar; Air Sea Interaction; Radar Clutter; Sea spikes; Remote Sensing

19. ABSTRACT (Continue on reverse if necessary and identify by block number)

Wind and wave data have been analyzed for the Panama City Tower Radar Experiment performed by Keller, Plant and Weissmann (1985), for comparison with radar data. Time series of wave height records were analyzed for a variety of definitions of wave height, with the resultant RMS heights calibrated against spectrum analysis results. As a result of the consideration of the wave spectra and wind history, the data are sorted into three types: equilibrium, fetch limited, and transient in time. Tracking the series of cross section-wind speed pairs for each data set over a few hour period indicates a well defined but different sequential development from one set the the next. While plotting of all the data produces the broad scatter previously reported, little scatter occurs about each individual track. This indicates that the specific sea surface characterization is primarily responsible for determining magnitudes of RCS, and that wind speed is only an implicit variable. Flow distortion effects are suggested as responsible for unusually high radar cross sections (RCS) previously reported for northerly winds, rather than atmospheric stability effects which were suggested originally.

20. DISTRIBUTION/AVAILABILITY OF ABSTRACT	21. ABSTRACT SECURITY CLASSIFICATION
☒ UNCLASSIFIED/UNLIMITED ☐ SAME AS RPT ☐ DTIC USERS	UNCLASSIFIED
22a. NAME OF RESPONSIBLE INDIVIDUAL Dennis B. Trizna	22b TELEPHONE (Include Area Code) (202) 767-2003 22c. OFFICE SYMBOL Code 5303

DD Form 1473, JUN 86 *Previous editions are obsolete.* SECURITY CLASSIFICATION OF THIS PAGE

S/N 0102-LF-014-6603 UNCLASSIFIED

CONTENTS

ANALYSIS OF ENVIRONMENTAL PARAMETERS FROM THE PANAMA CITY TOWER RADAR EXPERIMENT

INTRODUCTION

An experiment was conducted using an X-band radar on the Panama City Tower in the Gulf of Mexico, was reported upon by Keller, Plant, and Weissman (1985, hereafter referred to as KPW). In this paper the authors attempted to account for the variation of normalized radar cross section (NRCS) with wind speed, and to account for the departure from the predicted variation by considering effects of differences in air-sea temperature in the definition of wind friction velocity. This aim was based upon the assumption made in scatterometry that the large area NRCS of the sea is a function of wind speed to first order, and wind stress to next order, a parameter which reflects the variation in atmospheric stability. Relations between wind stress (τ), "air density (ρ)," wind friction velocity (u_*), and wind speed (U) are given by the following equations:

$$\tau = \rho u_*^2 \tag{1}$$

and

$$u_*^2 = C_D U^2 \tag{2}$$

which defines wind friction velocity in terms of measured wind speed, and where C_D is an empirically defined drag coefficient, which reflects effects of atmospheric stability through its airsea temperature difference dependence.

While such an empirical formalism is useful for engineering applications because it allows wind field estimates to be made from satellite radars over very large areas, it does not give insight into the primary sources of radar scatter from the sea for other applications. With other interests in mind, we have begun to re-analyze these radar data from three points of view: (1) definition of a new drag coefficient which provides a better air-sea temperature dependence than obtained by KPW; (2) investigation of the importance of specific characterizations of the sea surface on NRCS, rather than just wind speed; and, (3) processing the data in a manner similar to that used for non-coherent shipboard radars, for comparison with other experiments that we have conducted (Trizna, 1988).

As part of this general analysis, this report presents a comprehensive look at the environmental parameters collected on the tower. Wave spectra from a wave gauge are considered in detail, as well as the changes in wind speed and direction in the context of weather systems which passed through the area. Effects of flow distortion by the tower on the measurement of wind speed and its accuracy are discussed, and are suggested as the main reason for the departure of data from expected RCS-wind speed predictions. Other methods of analyzing wave data besides spectral analysis are also considered. Finally, consecutive files of data are considered as NRCS vs wind speed plots. These are shown to follow a tight track with time, with little scatter. It is concluded that scatter which does appear in the total plot of data is probably associated with non-unique sea surface characterizations which occurred due to non-fully developed conditions.

Manuscript approved November 13, 1987.

AIR AND SEA TEMPERATURES

Fig. 1 shows plots of air and sea temperature during the data runs. During this time, three outbreaks of cold air, or cold fronts, moved through the site, each one colder or more intense than the previous one. The fronts are identified in Fig. 1 by the sharp decreases in temperature. The air temperature is initially cooler than the sea temperature after the front passed the site, giving strongly unstable conditions. The air then gradually warms and ultimately causes a return to stable conditions. This condition persisted until the next cold front passed the site. Due to heat losses to the colder overlying air, the sea temperature decreased as the cold front passed the site. Indicated at the top of the figure is the start time of each run. The exact times are given in Table 1.

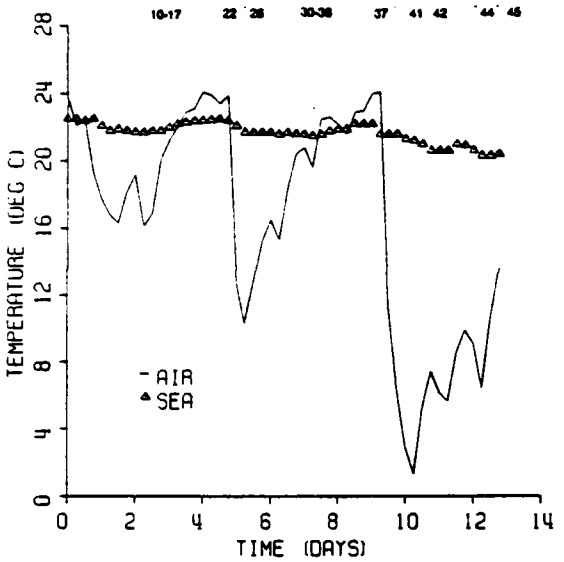

Fig. 1 — Temporal record of air and sea temperatures recorded during the experiment.

Runs 10-17 can be considered together since they are so close together in time. They cover the transition from negative to positive air-sea temperature differences after the first cold front. Similarly, runs 30-36 can also be taken together since they are also close together in time and cover a similar transition period after the second cold front. The other runs were taken separately under rather unique circumstances.

In runs 22 and 26, taken 5 & 16 hours respectively after the second cold front passed the site, the wind direction was opposite the wave direction and of limited fetch, having shifted to a northerly direction. Run 37, taken just as the third front passed the site, covered a change in air-sea temperature difference from positive to negative and again a wind-wave direction difference of 180 degrees. The last four runs were made after the third front passed the site, runs 41 and 42 when the air temperature had reached its lowest point and runs 44 and 45 two days later, when the air temperature had started to increase, but was still colder than the sea temperature.

WIND DIRECTION AND SPEED

Since wave development depends not only on wind speed, but also fetch, the direction of the wind and its duration are important. The wind directions are shown in Fig. 2. Each passage of cold air across the site was preceded by winds from the south west, with unlimited fetch. As the front passed, the wind shifted clockwise to the north, although it was initially west erly for the first front. After a period of time with northerly winds, depending on the movement of the front, the winds gradually shifted clockwise to the east and then to the south. As a result of this pattern, the fetch and

Table 1 — Start Time of Data Runs

Run	Data	Start Time
10	2 Dec	07:30
11		12:00
12		17:40
13		21:45
14	3 Dec	07:45
15		12:15
16		16:55
17		21:15
22	5 Dec	00:07
26		21:55
30	6 Dec	16:15
31		20:30
32	7 Dec	03:25
32		05:53
33		07:55
33		10:37
34a		13:15
34b		16:50
35		18:50
36	8 Dec	03:30
37	9 Dec	06:33
41	10 Dec	08:45
42		17:08
44	12 Dec	07:40
45		11:50

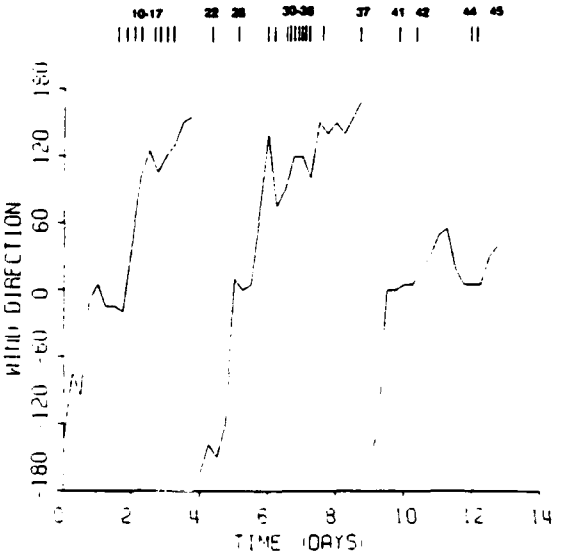

Fig. 2 — Temporal record of wind direction recorded during the experiment.

duration of the wind varied considerably for each of the runs (see Table 2). The wind speed during this period is shown in Fig. 3. Although not the case for the first front, the wind speed increased 12-18 hours before the passage of the second and third fronts. After the second front, the wind speed decreased, while after the third, it continued to increase. The reason for this behavior is possibly related to the greater temperature difference across the third front compared to the second (22°C vs 12°C) and its slow movement. In addition, all of the runs with the greatest atmospheric instability had winds from either the NNW(330°) or NNE(030°). This is expected to be the case for winter winds blowing off the colder mainland.

Table 2 — Fetch and Duration of Runs

Run	Fetch (Hz)	Duration (hrs)
10	41	3.5
11	56	7.5
12	41	14.5
13	56	18
14	104	24
15	185	11
16	185	16
17	185	12.5
22	21	4.5
26	37-185	2.5
30	56	15
31	56	17.5
32	37	27
33	65	32
34	140	22
35	110	15
36	148	23
37	185	26
41	15	22
42	15	30
44	15	31
45	15	30

Because of the unexplained high RCS values which were associated with the high air-sea temperature differences, further consideration of the geometry of the site are of use. The wind sensor was located at the south corner of the tower (the tower is in the shape of a square with the corners oriented north, south, etc.). It is strongly suspected that the wind sensor was in the wake of the tower for these wind directions, thereby giving erroneous wind speeds. Such effects have been reported in past experiments aboard the Argus Island tower (Thornthwaite, et al, 1985) and are to be expected with any tower.

Evidence for such behavior is shown in Fig. 4, which shows the distribution of wind speeds with azimuth angle for a two week period. The figure excludes any data used in the current analysis. The figure shows a decrease in wind speed for azimuths between 270-060 degrees, whereas one would expect the greatest influence between 270 and 090 degrees, since highest winds are encountered just after the passage of a front, tending to produce wind directions within such a sector. To counter the possibility that the wind speeds from these azimuths might have been naturally lower in magnitude because of the prevailing weather systems, shore based winds were also considered. Fig. 5 shows the distribution of wind speeds taken from a shore-based sensor ten miles away for the same time period. Although the speeds are not distributed uniformly with azimuth, there is no evidence of significantly lower wind speeds for azimuths between 270 and 090 degrees. This lends credence to

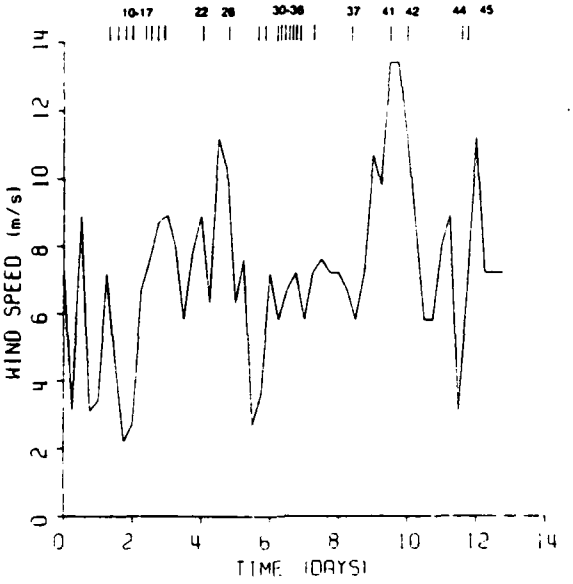

Fig. 3 — Temporal record of wind speed recorded during the experiment.

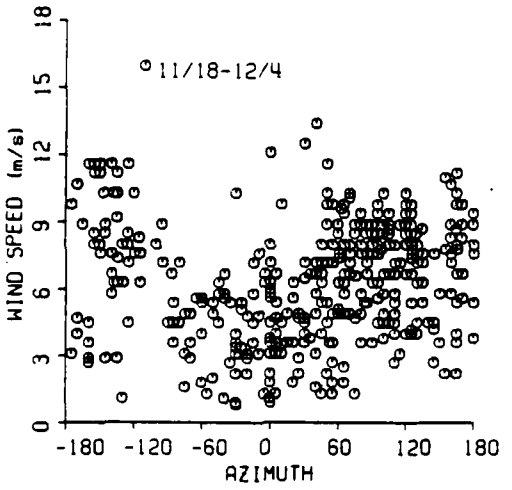

Fig. 4 — Measured wind speed versus azimuth angle recorded at the tower site for period 18 Nov - 4 Dec.

the suggestion that the decrease in wind speed in the wake of the tower is real. The magnitude of the effect is shown in Figs. 6a and 6b, which show the percent occurrence of wind speeds for two azimuth ranges, one not influenced by the tower (120-240 degrees) and the other in the wake of the tower (300-060 degrees). For azimuths between 300-060 degrees, the mode of the distribution occurs at 4.5 m/s, compared to a mode of 8.5 m/s for azimuths between 120-240 degrees. Thus, the measured wind speeds may be up to 4 m/s lower than the actual speeds. Plots of flow distortion effects by Thornthwaite, et al, indicate reductions in magnitude of as much as 30% for nominal heights on the back edge of Argus Island Tower.

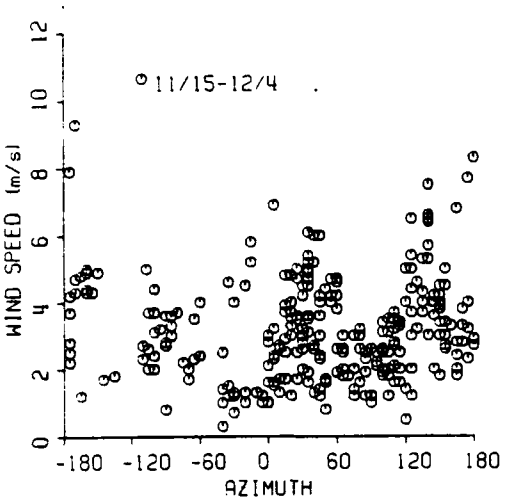

Fig. 5 — Measured wind speed versus azimuth angle recorded by shore-based sensor for period 15 Nov - 4 Dec.

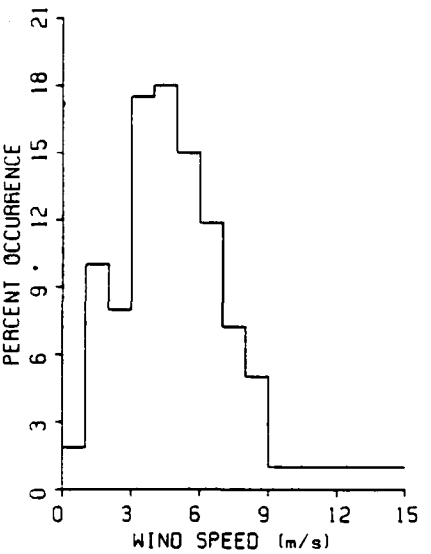

Fig. 6a — Wind speed distribution recorded at tower site for obstructed azimuth.

WAVE DATA ANALYSIS—TIME SERIES ANALYSIS

In addition to the meteorological data, wave heights were recorded from a wave staff mounted on the tower. Data were available for 12 of the 22 radar runs, which can be sorted into three different categories. These are as follows: runs (32-35), taken under relative steady-state or uniform conditions; four runs with short fetch (runs 41-45); and four runs (22,26,30 & 31) where conditions were transitory or changing with time. These runs will be discussed in more detail in the next section.

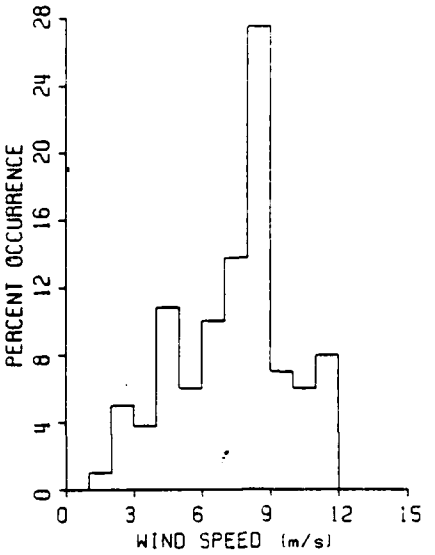

Fig. 6b. — Wind speed distribution recorded at tower site for unobstructed azimuth.

The wave gauge records were digitized at a sample interval of .32 seconds to provide an unaliased frequency of 1.56 Hz for spectral analysis. A Tektronix 7612D transient waveform analyzer was used for the digitization, with the tape replayed at 15 ips, eight times the original speed. For the 2048 data points of the record, the record length was 655 seconds or 10.9 minutes. In order to obtain a wave record comparable in length to the 21.3 minutes of the radar data, two consecutive records were combined to provide a record length of 21.8 minutes. The beginning of each 21.8-min period was aligned to begin at the same time as each of the radar records in KPW.

A single mean was determined for each 2048-point wave record and then subtracted to provide a zero-mean time series. Individual waves were defined by choosing a zero crossing in the negative direction as the start of a single wave, and the next negative down crossing as the end, and start of the next wave. The actual wave start was determined by interpolation between the last positive and the next negative digitized point. Similarly, an interpolated zero up-crossing point was determined and stored. An accurate minimum and maximum of each wave were determined with a three-point parabolic fit, stored as the peak and trough values, along with the fractional time value between each such point for each wave. From these values, the wave height, equal to the peak minus the trough values, and the slopes, according to several different slope definitions discussed in Trizna and Martin (1988) were determined and analyzed.

Calibration Techniques

Since amplitude calibration data were not available for the wave records, the wave heights were determined by equating the mean square amplitude from the time series to the integral of a theoretical saturated Phillip's spectrum (αf^{-5} for $f > f_{pk}$, 0 for $f < f_{pk}$, where f_{pk} is the peak frequency of the spectrum). From the available runs, a spectrum was chosen which came closest to being saturated, with a f^{-5} frequency dependence. However, it was taken under short fetch conditions, requiring modification of the expression for the Phillips constant, α, due tc a limited fetch according to Kitaigorodskii (1962):

$$\alpha = 0.076\, X^{-.22} \tag{4}$$

where X is a normalized fetch, $X = x_g / U_{10}^2$, and g is gravity. Integrating the theoretical Phillips' spectrum over the frequency range over which the observed spectrum followed a f^{-5} dependence provided a value for the mean square voltage amplitude. Then an amplitude scale factor was calculated, such that the mean-square/amplitude calculated from the time series equaled the value obtained from the integration of the spectrum. This scale factor was used to convert all of the digitized wave voltages to meters.

Definition of Statistics Terms

The wave statistics were determined by three different methods. Based on the work of Pierson, et. al. (1955), one can relate all of the wave height parameters to each other by the parameter E, where E is defined as twice the variance of a large number of wave amplitudes from points equally spaced in time. Based on Longuet-Higgins work (1952, L-H hereafter) the following relationships exist between E and the wave height parameters for a spectrum containing a narrow band of frequencies.

$$\text{Mean Squared Wave Height: } H^2 = 2E \tag{5}$$

$$\text{Root Mean Squared Wave Height: } H_{rms} = (2E)^{1/2} \tag{6}$$

$$\text{Mean Wave Height: } H = 1.77\,(E)^{1/2} \tag{7}$$

$$\text{Significant Wave Height: } H_{1/3} = 2.83(E)^{1/2} \tag{8}$$

From the time series, values of E were calculated using 4096-point records. From E, values of the significant wave height ($H_{1/3}$), the mean height and the root mean square height were determined. An alternative approach was to calculate the wave height statistics from the measured peak to trough wave heights, not assuming a narrow band spectrum. This was done for the zero down-crossing data described previously, with the height defined from the initial trough to the following peak. From the 21.8-min data record, approximately 300-400 individual waves were available. From the wave heights, the mean value and the average of the highest third were calculated. A third approach determined the wave parameters from the definition of the mean square wave amplitude as the integral of the spectrum and assuming the relationships between wave parameters as determined by L-H for a narrow band spectrum. In terms of the spectrum, assuming $A = H/2$ where A is the amplitude and H is the peak-to-trough height, the wave parameters are,

$$H^2 = 4\,[\int S(\Omega) d\Omega] \tag{9}$$

$$H = 2.5\,[\int S(\Omega) d\Omega]^{1/2} \tag{10}$$

$$H_{1/3} = 4\,[\int S(\Omega) d\Omega]^{1/2} \tag{11}$$

$$H_{rms} = 2\,[\int S(\Omega) d\Omega]^{1/2} \tag{12}$$

Figure 7 shows the correlation between H_{rms} calculated from the integration of the spectra and H_{rms} using the variance technique ($H_{rms} = (2E)^{1/2}$). The excellent correlation indicates the calculations are being done properly and gives confidence in the results. Figs. 8 and 9 show the correlation between the significant wave height ($H_{1/3}$) calculated as the average of the highest one-third waves versus $H_{1/3}$ calculated from the variance techniques and the spectrum, respectively. In both cases the correlation is excellent, with only a 7% difference between the various techniques. Fig. 10 shows the correlation between the significant wave height and mean wave height calculated directly from the time series, that is, not assuming the waves are narrowbanded. The ratio equals 1.55, in close agreement with the theoretical prediction of 1.6 by L-H and observed by many other workers.

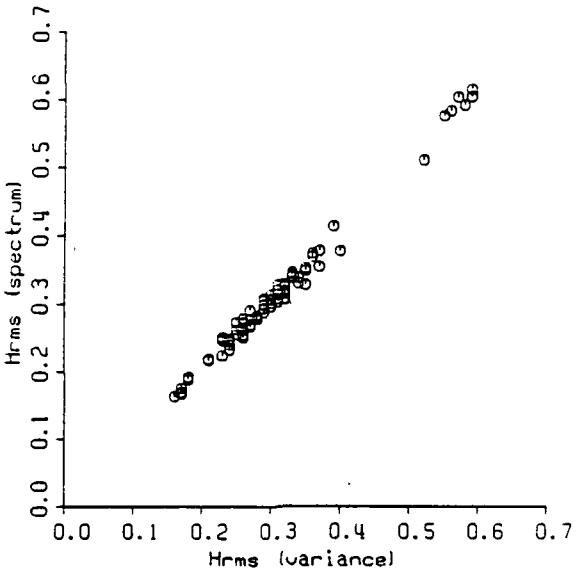

Fig. 7 — H_{rms} calculated from spectrum versus H_{rms} calculated from variance of the time series.

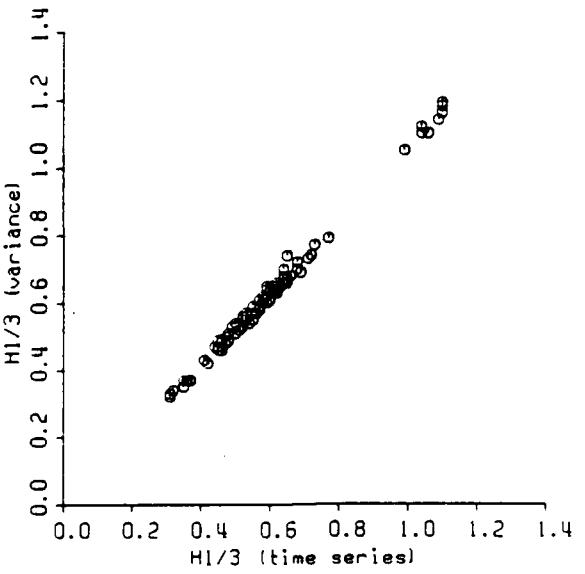

Fig. 8 — $H_{1/3}$ determined from variance of time series versus $H_{1/3}$ calculated from average of one-third highest waves.

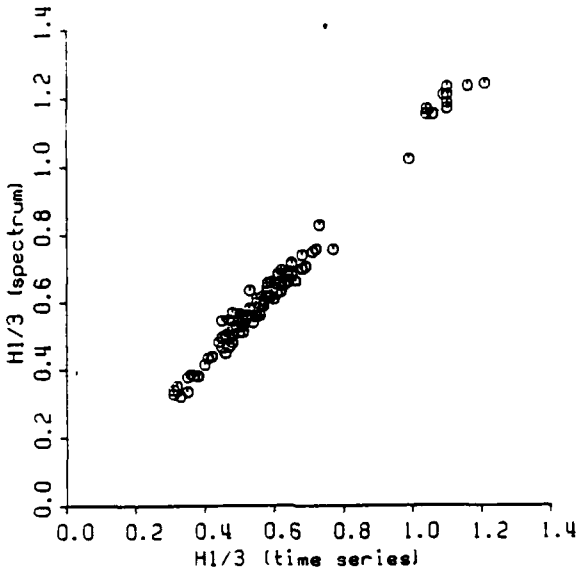

Fig. 9 — $H_{1/3}$ determined from wave spectrums versus $H_{1/3}$ calculated from average of one-third highest waves.

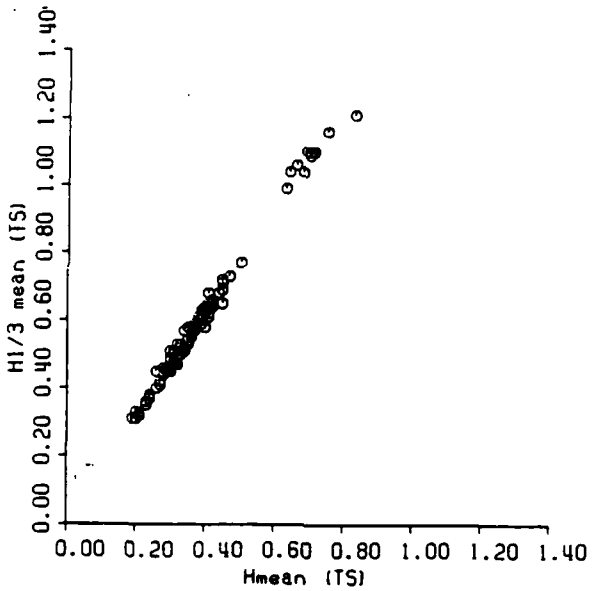

Fig. 10 — H_{rms} versus H_{rms} determined from the time series.

As an indication of the distribution of waveheights, the spectral width parameter, defined by

$$SW^2 = 1 - (N_z/N_c) \tag{13}$$

was calculated for the various runs. In this expression, N_z is the number of positive zero crossings during the run and N_c is the number of crests, which may be above or below the mean value. Typical values were near 0.8, where $SW^2 = 0$ would be expected for a Rayleigh distribution of wave heights and $SW^2 = 1$ is the expected value for a Gaussian distribution. The observed height distribution for two cases are shown in Fig. 11. Run 22/1 is for the case for the highest waves observed, a case with a well developed sea, followed by a frontal passage with the wind coming from the opposite

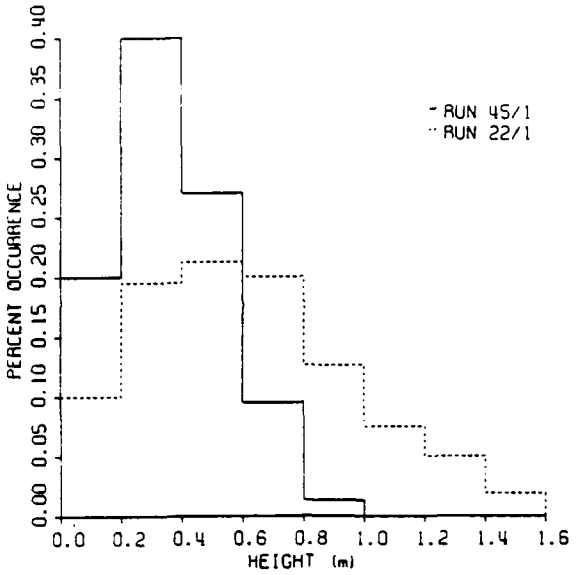

Fig. 11 — Wave height distributions for two sea conditions; a well-developed sea state (run 22/1) and a fetch-limited case (run 45/1).

direction and increasing over the run. Run 45/1 shows the distribution of heights for short fetch conditions after sufficient time had passed so as to eliminate the longer (and therefore higher) waves. The final figure in this section (Fig. 12) shows the significant wave height versus the median period of all of the observed waves. The solid line is the prediction of Schmied (1985) based on the Pierson-Moskowitz spectrum and sets an upper limit for the observed points. This is not unexpected since neither time nor fetch was sufficient to allow growth of a fully developed sea state.

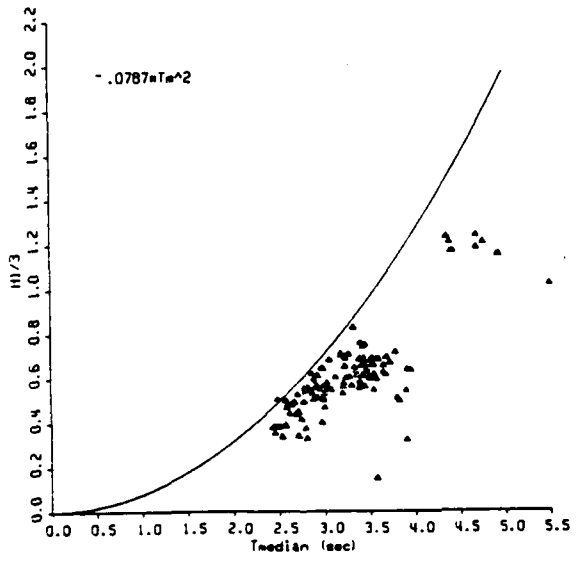

Fig. 12 — Significant wave height (H_{sig}) versus median wave period.

WAVE DATA—SPECTRUM ANALYSIS

The time series from the digitized wave data were also subjected to Fourier analysis to obtain wave height variance spectra. Using a 256 point FFT calculation with Hamming weighting, the coherent integration time was 81.92 seconds, resulting in a spectral resolution of 0.0122 Hz. Time overlap was utilized in processing the data. That is, after a 256 point record was processed, the last 128 points of the record were shifted to the first 128 input points of the new record and next 128 points were used to fill the second half of the new input record. Such time overlap effectively provides nearly independent spectra because of the severe weighting of the data points near each end of the time series. Thus, for a 4096 point record, 31 spectra were calculated. These were incoherently summed to provide an averaged spectrum for the 21.84 minute period. Peak frequencies were determined from the averaged spectrum for the wind driven portion and swell. This period was slightly different than that used in KPW, which required a readjustment of the start time of each record of 4096 points in the digitization process.

Amplitude Calibration of Spectra

The scaling of the spectra was done in a different manner from that of the time series, because of properties of the FFT software requiring digital input data, the raw digital data used in this case. The Phillip's asymptote, in square meters per Hz, is given by

$$S(f) = 0.0081\,(2\pi)^{-4}\,g^2 f^{-4} \tag{14}$$

$$= 5 \times 10^{-4}\,(m^2/Hz) \tag{15}$$

Thus, at one Hz, S(f) equals -33 db m^2/Hz. Using the same run that was used to determine a decibel scaling factor for wave height, the saturated spectrum was adjusted so that it equaled -33 db m^2/Hz at 1 Hz. Because the test spectrum was a fetch limited case, adjusting the fetch dependent parameter as before changed the actual value to -31 dB m^2. Once the adjustment factor was determined for this spectrum, the same factor was applied to all of the remaining spectra. The emphasis of the following discussion of wave spectra is directed toward the temporal changes in spectral characteristics due to changes in environmental parameters, for purposes of classifying the data into groups for comparison with radar data in Trizna and Martin (1988). As a result of this emphasis and the general lack of fully developed spectra, little discussion is provided as to agreement of the data with various models.

Characterization of Waves for Various Data Runs

Run 22 - As noted in the background discussion, run 22 was made five hours after the second cold front passed the site. For eighteen hours previous to the passage of the cold front, the wind direction was from the southwest, where the fetch was unlimited (see Fig. 13). The wind speed during this time varied from 6.5 to 12 m/s. As the front crossed the site, the wind direction shifted to the north, reducing the fetch to 11 miles. Temporarily ignoring the effect of the wind shift, one would expect a relatively smooth single-peaked spectrum with the peak corresponding to that predicted from the wind speed. The average of the first three 20 minute spectra, shown in Fig. 14, is a smooth spectrum with a peak at .17 Hz. Using $f_{pk} = 1.48/U$ where U is the wind speed in m/s, the frequency peak corresponds to a speed of 8.6 m/s, close to the mean wind value over the previous eighteen hours. The wind, after having shifted direction with frontal passage five hours previous to the run, increased in speed from 7.0 to 11.5 m/s during the run, before decreasing slightly. The response of the spectra to these changes are shown in Fig. 15, which shows the average of the first and last three 20 minute spectra. Only minor variations near 0.2 Hz are evident and these are not considered

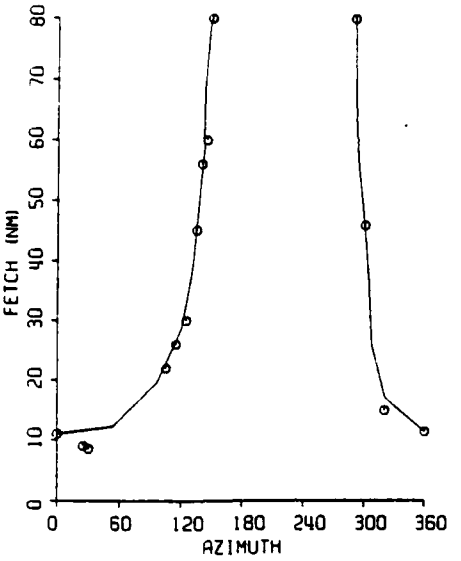

Fig. 13 — Fetch in nautical miles versus azimuth angle for Stage 1 tower site.

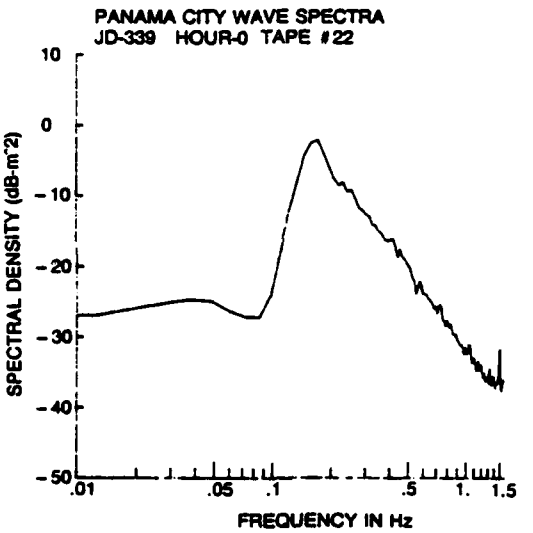

Fig. 14 — Averaged spectral density for first hour of run 22.

significant. However, the spectra are not saturated, or follow a f-5 dependence, even at high frequencies. One might speculate that this is a consequence of the wind direction being opposite the wave direction from the previous winds. The mean square wave height, proportional to the total wave energy and shown in Fig. 16, increases slightly over the run. However, the peak frequency (see Fig 16) remains roughly constant through the period (ignoring the third to the last point as a fluctuation).

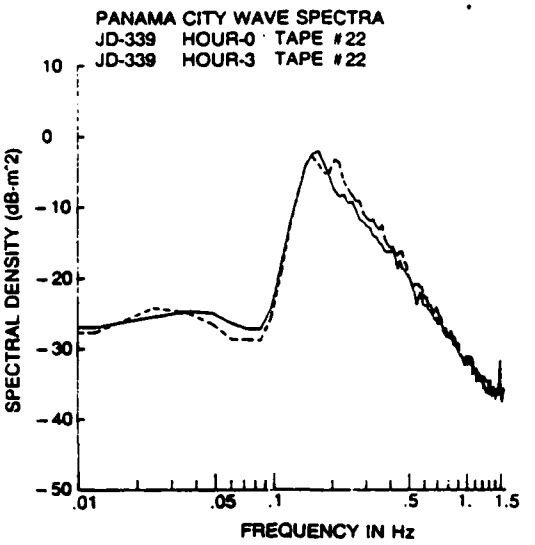

Fig. 15 — Change in spectral density between first and last hours of run 22.

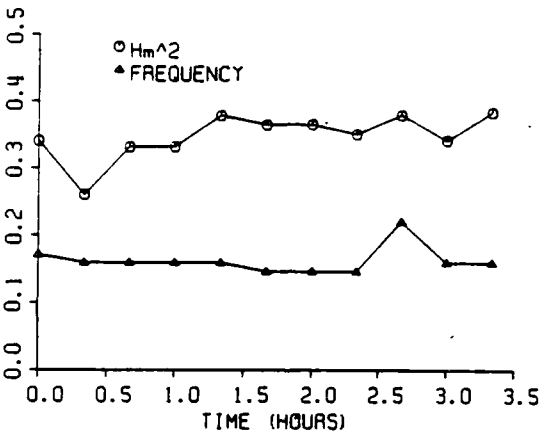

Fig. 16 — Temporal record of mean square wave height and peak frequency of wave spectrum for run 22.

The observed wave heights for this run are two-three times larger than heights observed during any of the other runs. There are several reasons for this: (i) the time and fetch available for wave growth before frontal passage; (ii) the 4.5 m/s increase in wind speed over the run; (iii) the interaction between waves propagating in opposite directions; and, (iv) the effect of the wind blowing opposite the waves. Complicating the situation even further is the unstable atmospheric conditions that prevailed after the cold front passed the site, and evidence that the wind sensor was sheltered for wind directions from the north, causing the observed wind speeds to be too low. This run might be expected to produce quite anomalous radar results due to the confused seas expected.

Run 26 - This run was made 24 hours after run 22. The wind direction, having persisted from the north for 20 hours, shifted to the southeast six hours previous to the run (see Fig. 2). Concurrently, the wind speed decreased from a maximum of 14.5 m/s shortly after run 22 to a minimum of 2 m/s nine hours later, gradually increasing to 6 m/s at run time. Fig. 17 shows the average of the last three 20-minute spectra for run 22, compared to the average of the first three 20-min spectra for run 26. There is a large decrease in wave energy for frequencies between generated by the southwest

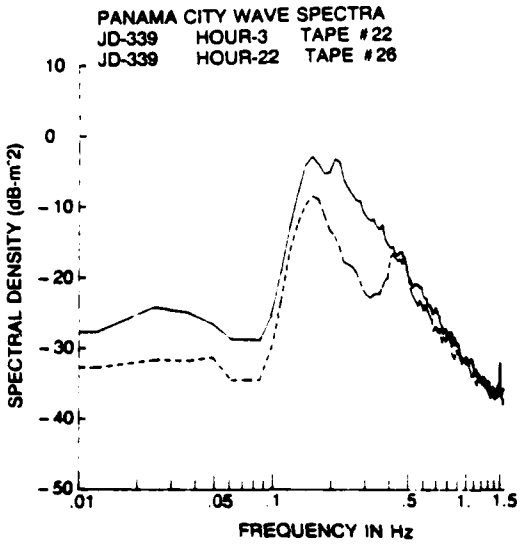

Fig. 17 — Change in spectral density between last hour of run 22 and first hour of run 26.

airflow prior to run 22 propagating beyond the site and contributing less and less to the spectrum. The energy at 0.5 Hz and higher is presumably locally wind driven, yeilding a dual-peaked spectrum, with peaks at .42 Hz and .15 Hz. Separation of the wave height into sea (waves traveling into the area from previous winds) and locally wind generated waves (assuming a cutoff frequency of .5 Hz), shows that the sea made up a significant portion of the total wave height (80% initially to 67% at the end of the run). Hence, one would not expect the radar return to correlate well with these winds. During the run, the wind speed varied only ±1 m/s about a mean value of 6 m/s. The change in the spectra, see Fig. 18, shows significant growth of wave energy between 0.3 to 0.4 Hz, and no loss for frequencies less than .2 Hz. This is reflected in the decrease in peak frequency from .46 to .34 Hz (see Fig 19).

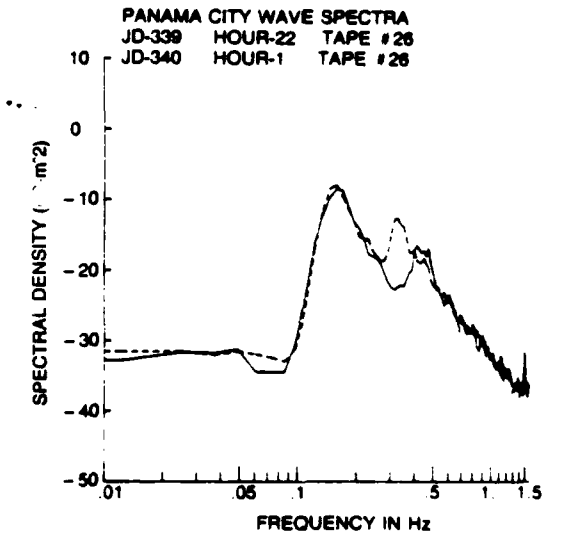

Fig. 18 — Change in spectral density between first and last hours of run 26.

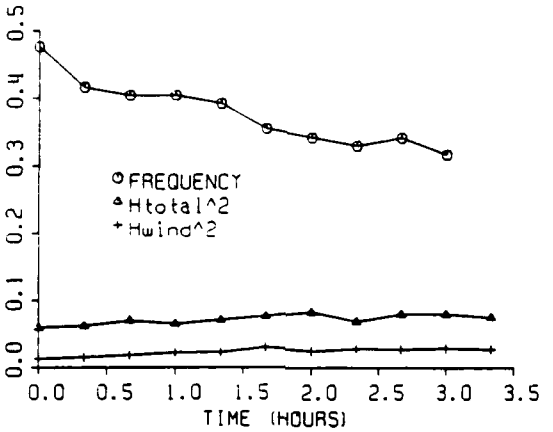

Fig. 19 — Temporal record of mean square wave height (total height and the height due to wind waves alone) and peak frequency of wave spectrum for run 26.

Run 30 - This run was made 18 hours after the previous run. During this period, the wind direction shifted from the south back toward the east, with the speed remaining near 7 m/s. The change in the spectra from run 26 to run 30 is shown in Fig. 20. It shows a loss of wave energy for all frequencies less than .6 Hz. This run produced the lowest wave heights observed during any of the runs, a result of the previously generated waves propagating beyond the site and the weak air flow with short fetch failing to produce any wave growth. At the start of the run, the sea component made up 44% of the total wave height. Shortly before the run started, the wind speed decreased to 4 m/s. From this speed, it increased steadily to 9.3 m/s by the end of the run. The change in the spectra, shown in Fig. 21, shows a significant increase in wave energy between .2 and 1. Hz. The growth starts at high frequencies and gradually shifts to lower frequencies with time. In addition, wave energy continues to decrease at low frequencies. The wave height, shown in Fig. 22, does not change significantly for the first 40 minutes, after which time it steadily increases. The peak frequencies, also shown in the same figure, show a sharp drop from .33 to .27 Hz after 40 minutes and then slowly decrease thereafter (ignoring the last data point). The behavior of the spectra during this run is consistent with what one would expect from the increase in wind speed, that is, a large increase in wave height. One reason why the wave development behaves as expected this case is the elimination of waves from the previous southwest airflow. Therefore, the wind was starting with a relatively "clean slate."

Run 31 - This run was made four hours after run 30. The wind direction remained from the east-southeast, but the speed varied, initially decreasing, then increasing before decreasing again. The temporal changes in wave height and frequency peak are shown in Fig. 23. The wave height shows a gradual decrease, consistent with the decrease in wind speed. The frequency peak remains relatively steady over the run. These results are consistent with the minor changes in spectral shape that were observed, both between this run and the previous one, and during the run itself.

Runs 32, 33,34 and 35 - These runs are considered together since they were made under similar environmental conditions; the wind speed was close to 7 m/s and the direction was from the southeast. These runs were made four hours after run 31 and were made immediately following one another. The environmental conditions were as close to steady-state as occurred during any of the runs; that is the fetch was sufficiently long (greater than 60 miles) and the wind speed was steady. A typical spectrum (the average of three 20-minute spectra) is shown in Fig. 24. The peak occurs at a frequency of 0.2 Hz, close to the predicted value for a wind speed of 7.4 m/s. This value is unchanged between any of the spectra. This constant frequency peak is consistent with the minor variations in spectra that were observed, either between the various runs or within individual runs.

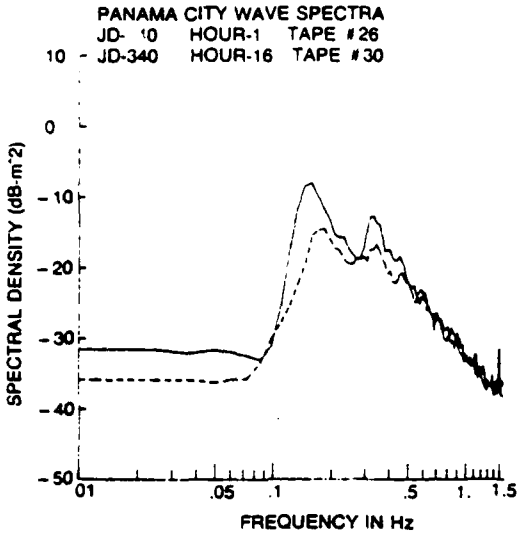

Fig. 20 — Change in spectral density between last hour of run 26 and first hour of run 30.

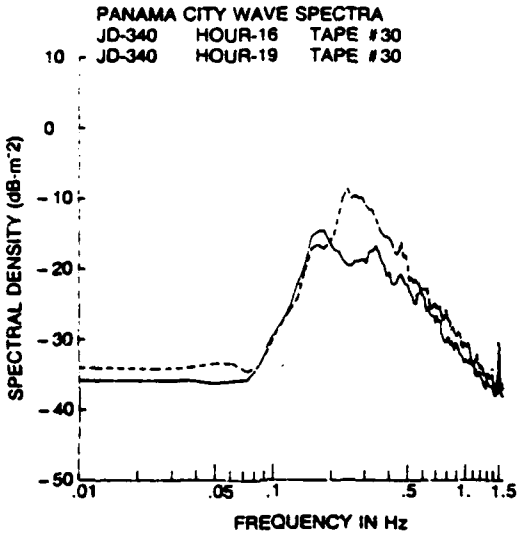

Fig. 21 — Change in spectral density between first and last hours of run 30.

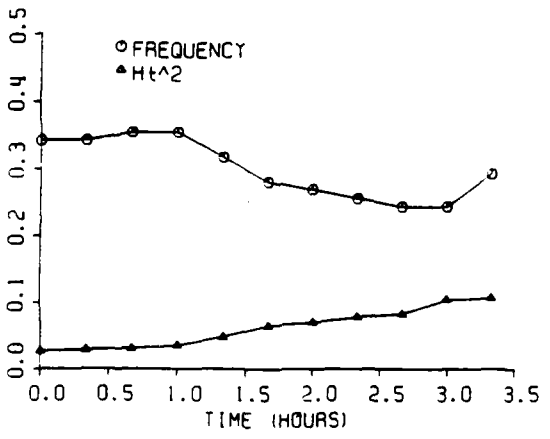

Fig. 22 — Temporal record of mean square wave height and peak frequency of wave spectrum for run 31.

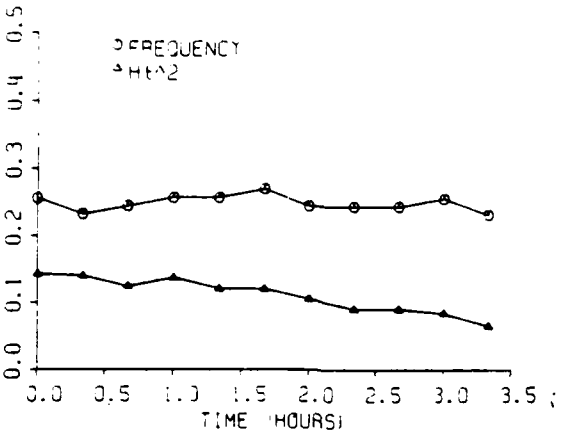

Fig. 23 — Temporal record of mean square wave height and peak frequency of wave spectrum for run 31.

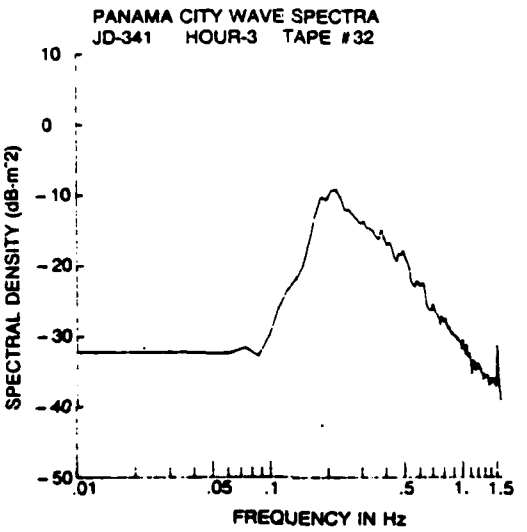

Fig. 24 — Spectral density for the first hour of run 32.

Consequently, the corresponding values of wave height were also unchanged during the runs. Although the observed spectral peak agrees with that predicted by the wind speed, the spectra are not saturated.

Runs 41-42 - These runs, taken 24 hours after the third cold front crossed the site, are considered together because they were made under similar conditions. Between runs 35 and 41, significant changes occurred in the wind. After run 35, the wind continued its clockwise shift in direction, gradually moving to southwest and increasing in speed. As a result, the wind direction was within 30 degrees of southwest (with unlimited fetch) for 10 hours before frontal passage. Based on these conditions, one might expect a spectrum similar to the one observed in run 22, which also had southwest airflow before frontal passage. The average of the first three 20 minute spectra is shown in Fig. 25. Instead of a single-peaked spectrum, the spectrum is dual-peaked, with peaks at .13 and .28 Hz. However, the spectrum is close to saturation for frequencies greater than .28 Hz. The change in spectra between runs 35 and 41 is shown in Fig. 26. There is decrease in wave energy between .15 and .23 Hz and a gain of energy for frequencies less than .15 Hz. This behavior is consistent with earlier development of a single peaked spectrum by the southwest airflow before frontal passage, and its decay as the wind shifted to the north and was opposite the wave direction. Also of importance

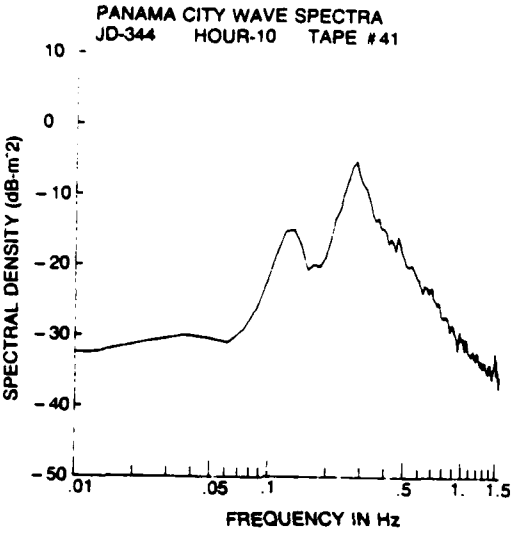

Fig. 25 — Spectral density for the first hour of run 41.

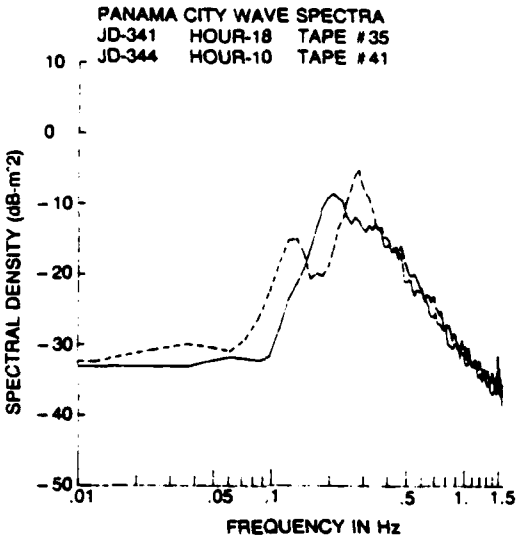

Fig. 26 — Change in spectral density between last hour of run 35 and first hour of run 41.

are the longer time (and effective fetch) of southwest airflow before frontal passage in run 22 compared to run 41 (19 hours vs 10 hours), and the time differences between frontal passage and the time of the runs (5 hours vs 24 hours). The change in the spectra during the run, shown in Fig. 27, shows the continued loss of wave energy for frequencies between .15 and .28 Hz, with the frequency peak shifting to higher frequency (see Fig. 28). This trend is also evident in the behavior of wave height, which also decreases with time (see Fig. 28). The reason why the spectra are close to saturation for this run and not run 22 is probably due to the longer time the wind blew from the same general direction in this case, as is apparent in Fig. 2. In addition, there is a greater instability associated with the third front compared to the second (T_{air}-T_{sea} equals -23°C vs -12°C, respectively). Run 42, made four hours after run 41, shows no significant changes from run 41 or changes with time. This is consistent with the observed steady values of wave height.

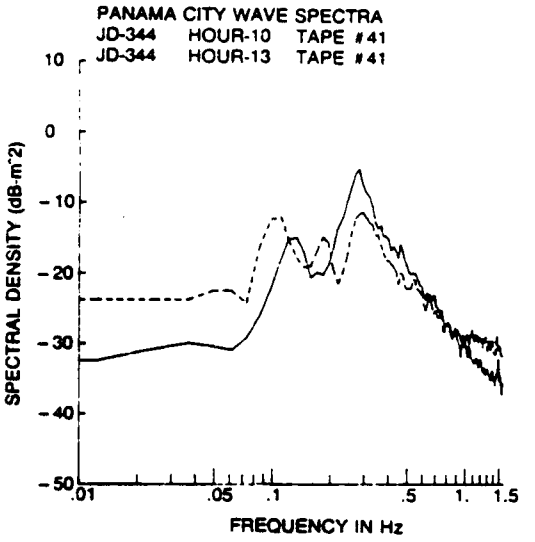

Fig. 27 — Change in spectral density between first and last hours of run 41.

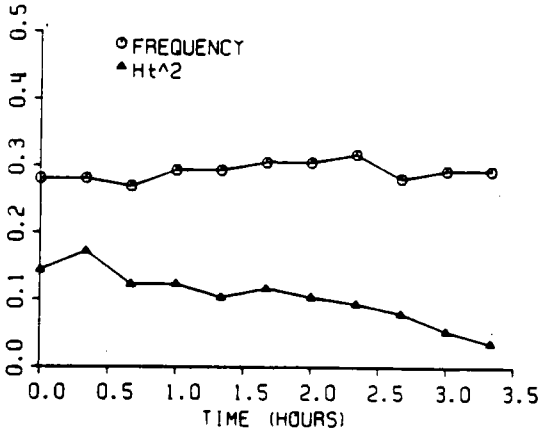

Fig. 28 — Temporal record of mean square wave height and peak frequency of wave spectrum for run 41.

Runs 44-45 - Between runs 42 and 44, an additional 24 hours passed. During this time, the wind shifted to the northeast and then back to the north, still providing short fetch conditions. The speed varied as well, first decreasing to 3 m/s, then increasing to 12 m/s before decreasing to 7 m/s by run time. Fig. 29 compares spectra from runs 42 and 44. There is no change for frequencies greater than .28 Hz, a gain of wave energy between .18 and .28 Hz and a significant loss for frequencies less than .18 Hz. The loss for low frequencies is part of the continuing loss of waves generated by the southwest airflow before frontal passage as they pass beyond the site. The gain in wave energy around .2 Hz can be associated with the increase in wind speed. The change in the spectra over the run are shown in Fig. 30. This change is reflected in the change in the wave height, which decreased slowly over the run, shown in Fig. 31. This is independent of the wind speed, which showed no variation over the run. Run 45, taken immediately following run 44, shows only minor changes in spectral shape from run 44. However, there is a continuous loss of wave energy for frequencies less than .33 Hz (see Fig 32). This is consistent with the decrease in the peak frequency and the continuous decrease in the wave height (see Fig. 33). The reason for the sudden loss of wave energy during this run after the unchanging conditions of run 44 are unknown.

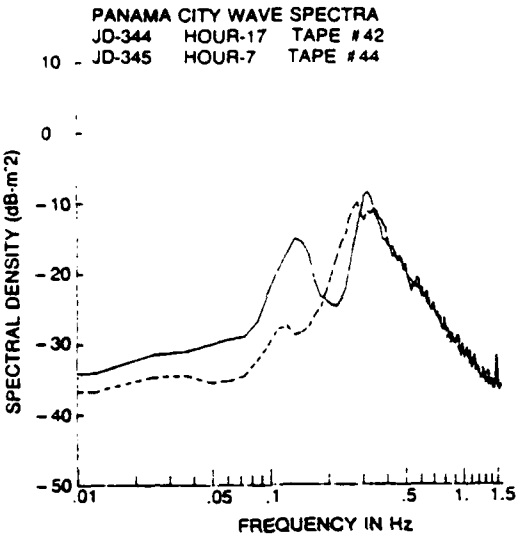

Fig. 29 — Change in spectral density between the first hour of run 42 and first hour of run 44.

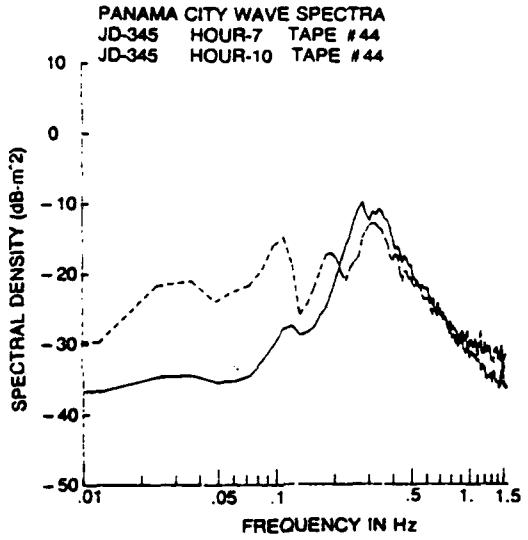

Fig. 30 — Change in spectral density between first and last hours of run 44.

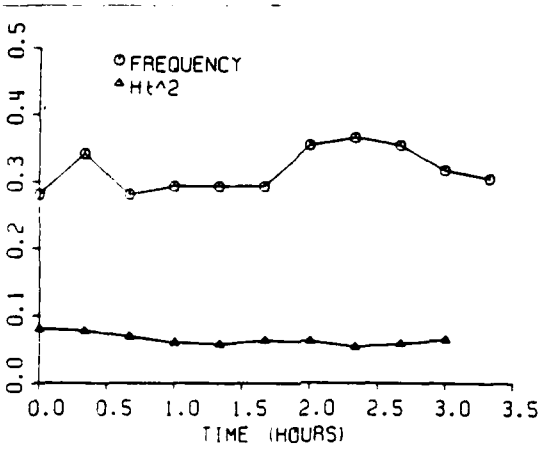

Fig. 31 — Temporal record of mean square wave height and peak frequency of wave spectrum for run 44.

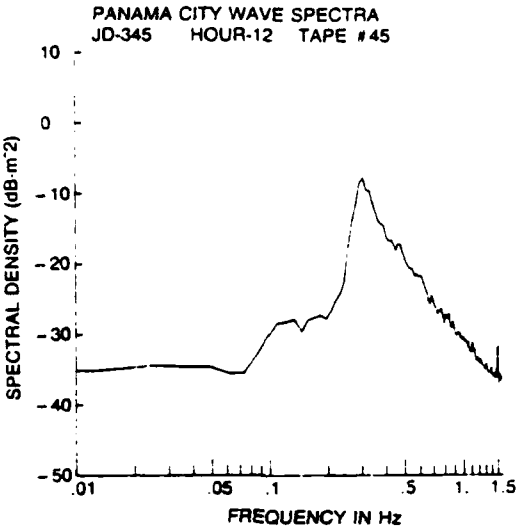

Fig. 32 — Spectral density for first hour of run 45.

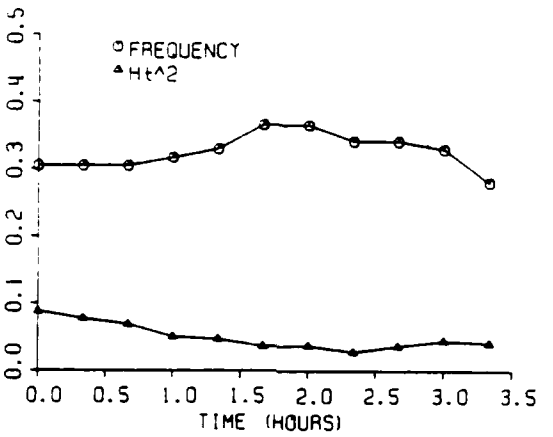

Fig. 33 — Temporal record of mean square wave height and peak frequency for run 45.

TEMPORAL DEVELOPMENT OF RCS WITH TIME

While the original plot of RCS vs wind speed in KPW showed a reasonable amount of scatter about their fitted $u^{2.3}$ curve, it was noted that a given sequence of RCS values with time followed a rather narrow track near the same curve, with very little scatter. Fig. 34 shows examples of four of such occurrences for which the RSC varied significantly over a run, but for which no in-situ wave records existed. While not specifically labeled in their sequential order, the nearest neighbor for each different plot symbol indicates sequential points in time as well, and it is clear that the RCS-wind speed temporal development follows a very regular path in each case. It is postulated that the narrow track is a result of the regular and continuous development of the wave system, including both the decay of the swell and the response of the wind waves to local winds.

If true, it follows that the spread in the KPW RCS-wind speed summary curve is due to slightly different characterizations of the sea surface due to waves present from previous winds, so called sea and swell. This hypothesis would indicate that the wind speed is an implicit variable for an RCS comparison, through its development of the wave system responsible for the radar scatter. Hence, any condition in which waves continue to run due to a previous wind direction, with sufficient time

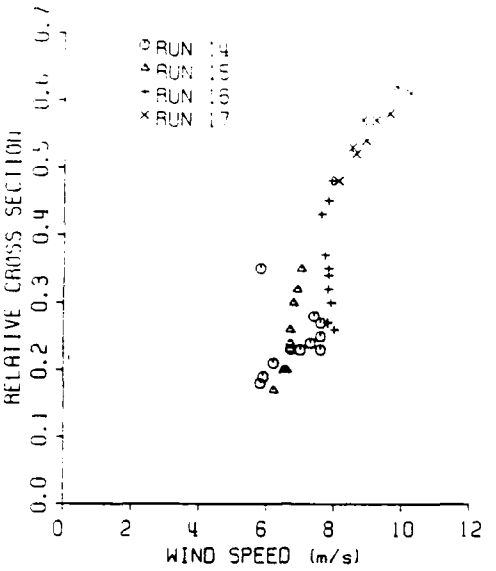

Fig. 34 — Relative radar cross section versus observed wind speed. Note the small variability for individual runs.

and fetch to allow a bi-modal spectrum to develop, would probably produce an offset or error of RCS-wind speed correlation relative to winds which generate a single-mode wave spectrum.

Let us investigate this hypothesis further by considering the wind and RCS tracks in time for each of the runs of the three sets defined in the previous section, for which wave records existed. Figures 35a-d show plots of relative RCS and wind speed for the equilibrium set of data and these indicate relatively good correlation with wind speed. The differences in the plots for the two curves it quite similar for these data. Figs. 36a-d show similar results for the fetch limited data. Relatively good correlation exists again, but with a different scaling in RCS vs wind amplitude, the RCS being significantly higher. (The last run shows poorer correlation for reasons unknown at this point in our analysis.) Finally, the four cases of non-equilibrium transient conditions are shown in Figs. 37a-d, and show the worst correlation. The first of these, run 22, occurred nearest in time after the 180-deg change in wind direction, with significant swell continuing to run from the previous wind direction. It shows the worst correlation of the group on a relative basis between RCS and wind speed of the set of four, as might be expected from significant swell running opposite the wind, with little time allowed for the waves to respond to local winds.

SUMMARY

In this work we have processed environmental parameters collected for the Panama City Tower experiment reported on by Keller, Plant, and Weissman (1985) in preparation for further analyses of these data. In particular, wave staff data collected on the tower have been analyzed using both spectral analysis and time series analysis, with calibrations detailed for both. With the onset of spectral analysis of wave data, the use of time series analysis has generally fell into disuse. However, recent studies on correlating wave breaking occurrence with local wave steepness (Holthuijsen and Herbers, 1985) have renewed our interest in the use of time series of the surface profile as a radar comparison tool. For this reason, the various definitions of significant, rms, mean, and highest 1/3 heights are stated for time series processing. The definitions of significant wave height were compared for the two different processing techniques and results were very good, reinforcing our confidence in the time series technique.

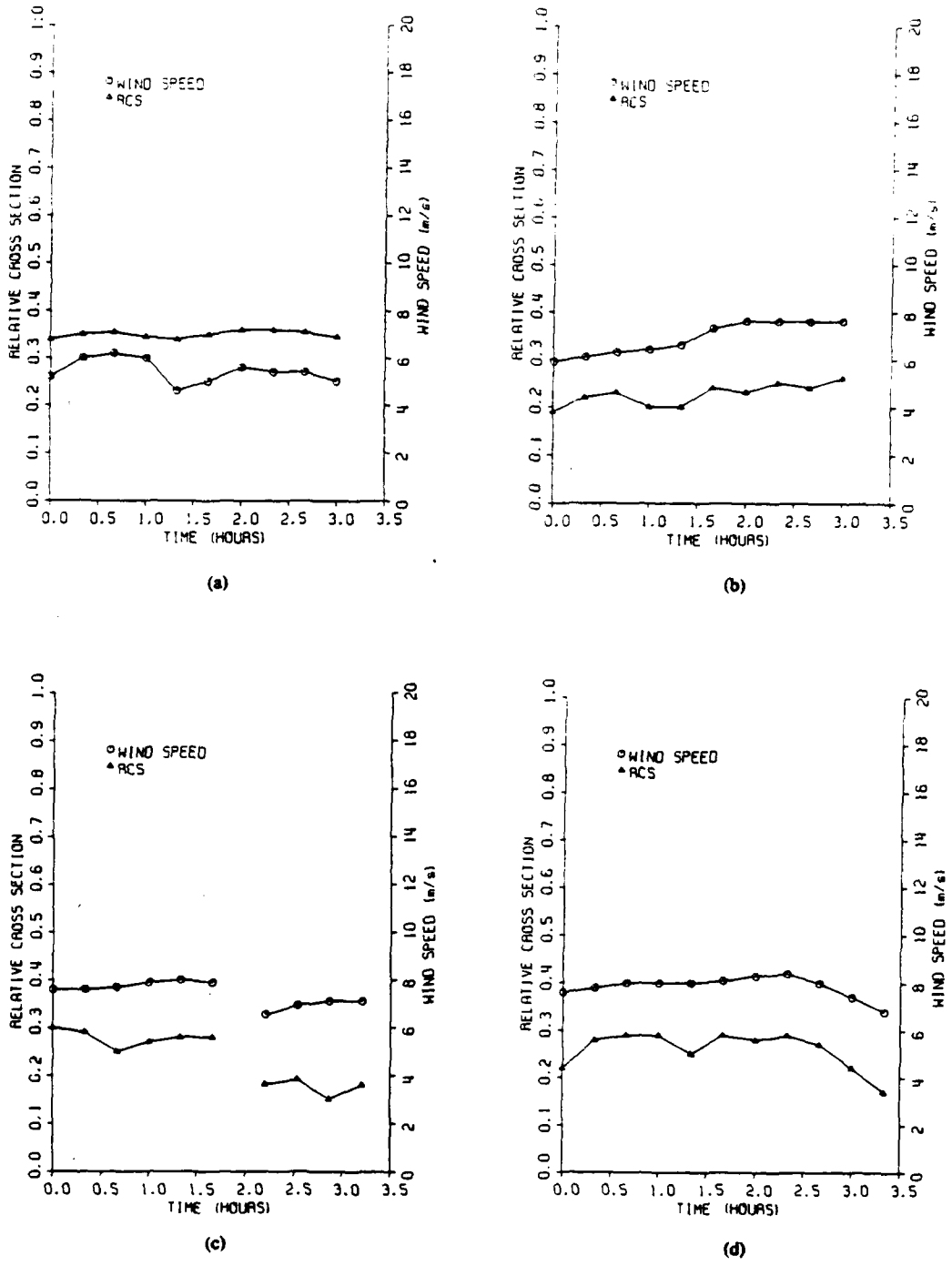

Fig. 35a-d — Relative cross section versus time for equilibrium runs.

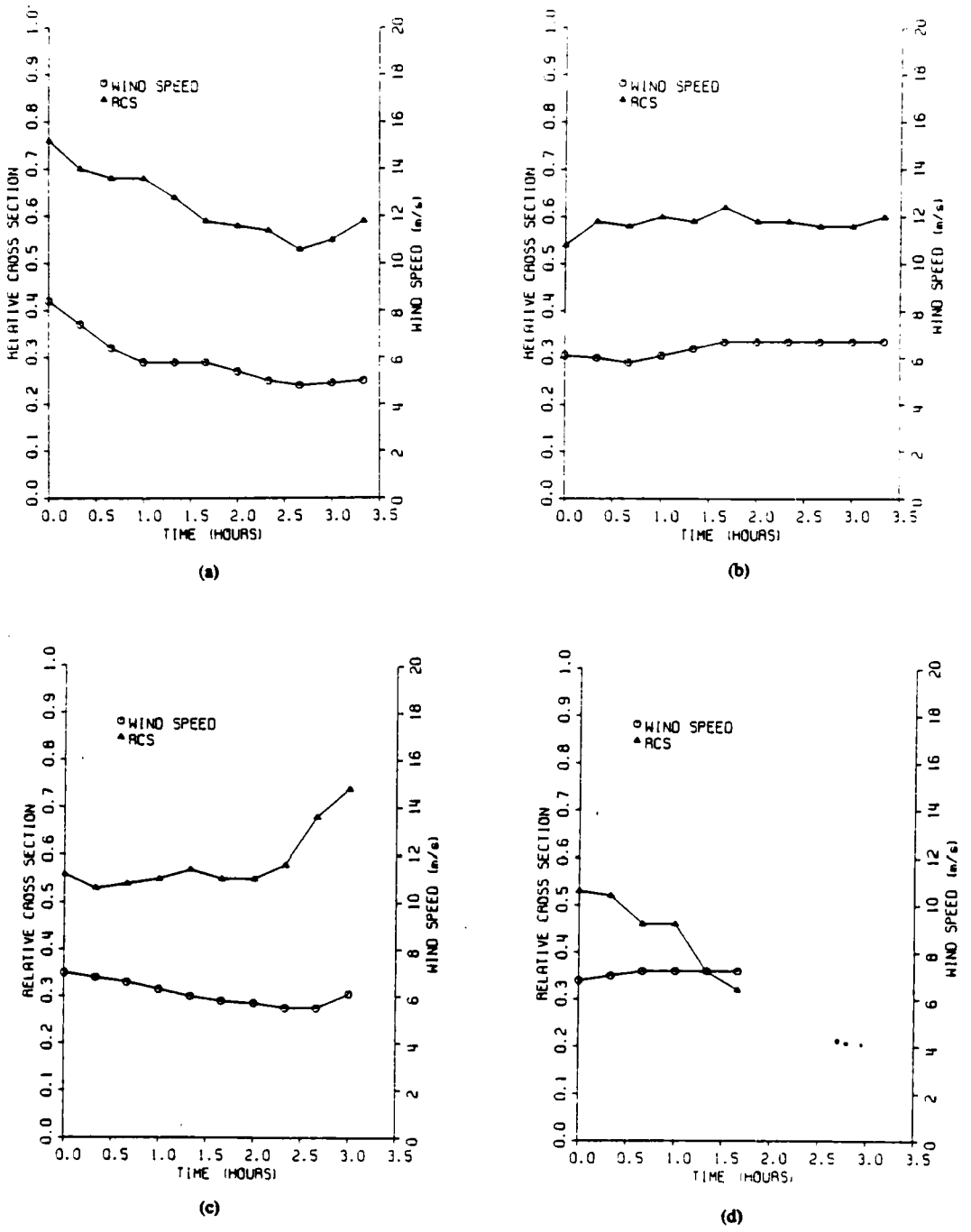

Fig. 36a-d — Relative cross section versus time for fetch limited runs.

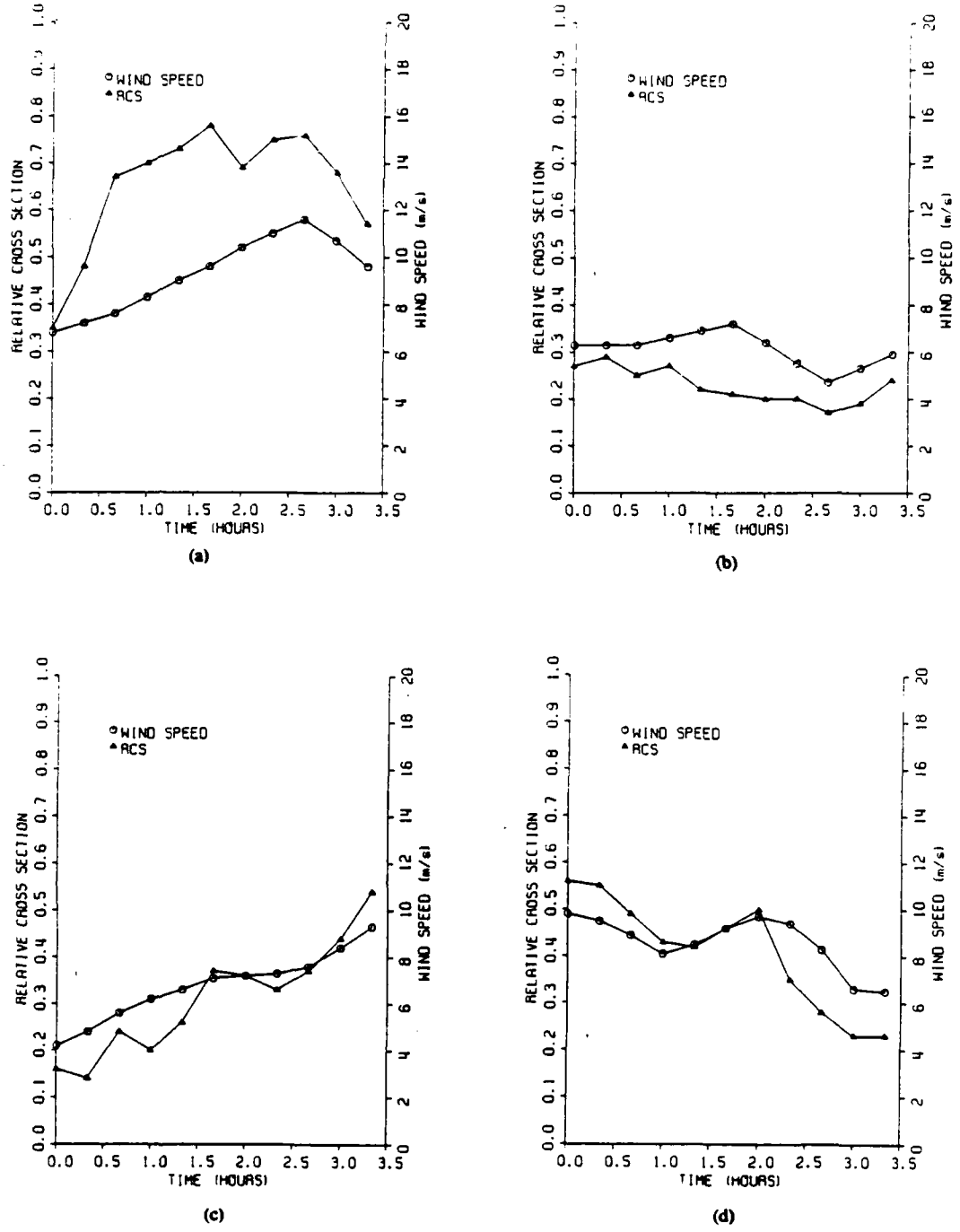

Fig. 37a-d — Relative cross section versus time for non-equilibrium runs.

The twelve sets of data for which wave staff data existed were processed, and a variety of environmental parameters were displayed. Based on the time histories of the wind, these were divided into three groups and characterized as (1) equilibrium, (2) fetch limited, and (3) transient conditions.

Several examples of the changes in RCS and wind speed from one twenty-minute data run to the next were shown, in which it was noted that the track from one time period to the next show continuous development, with very little random scatter from one period to the next. It was hypothesized that the reason was that the specific sea surface characterization played a dominant role in determining the RCS value, and that the wind speed correlates only as an implicit variable, which generates the wave conditions. For cases of swell or changing wind directions, one expects poor RCS-wind correlation. Individual plots of wind speed and RCS versus time show similar characteristics for the three groupings of wave conditions defined above, with poorest correlation for transient conditions, lending credence to our hypothesis.

In the future, the radar data will be compared with a variety of definitions of long wave slope and newly defined drag coefficients for wind stress determination and comparisons, which will account for both atmospheric stability and the presence of swell.

ACKNOWLEDGEMENTS

We wish to thank Bill Keller and Bill Plant for graciously making available the Panama City Tower radar data tapes for our use. We also wish to acknowledge our discussions with Professor Jin Wu, of the University of Delaware on the subject of processing of wave records and generally enlightening and stimulating ideas on the subject, and John Fahnestock and Tad Blanco for helping with development of software and running programs for the display of the data.

REFERENCES

1. Holthuijsen, L.H. and T.H.C. Herbers, "Studies of breaking waves observed as whitecaps in the open sea," J. Phys. Ocean., Vol. 16, pp. 290-297, 1985.

2. Keller, W.C., W.J. Plant, and D.E. Weissmann, "The dependence of X-band microwave sea return on atmospheric stability and sea state," J. Geophys. Res., Vol. 90(C1), pp. 1019-1029, 1985

3. Kitaigorodskii, S.A., "Applications of the theory of similar ity to the analysis of wind-generated wave motion as a stochastic process," Bull. Acad. Sci. USSR Geophys. Series1,73, 1962.

4. Longuet-Higgins, M.S., "On the statistical distribution of the heights of sea waves," J. Marine Res., Vol 11(3), pp. 245-266, 1952.

5. Pierson, W.J., G. Neumann, and R.W. James, "Practical Methods for observing and forecasting ocean waves," H.O. Pub603, U.S. Navy Hydrographic Office, pp. 6-11, 1955.

6. Schmeid, L., "Sea state cycles," in The Ocean Surface, Y. Toba and H. Mitsuyasu (Ed.), D. Reidel, Dordrecht, Holland, 1985.

7. Thornthwaite, C.W., W.J. Superior, and R.T. Field, "Disturbances of airflow around Argus Island near Bermuda," J. Geoph. Res, Vol. 70, pp.6047-6052, 1965.

8. Trizna, D.B. and L.U. Martin, "Definitions of long ocean wave slope for radar applications," NRL Memorandum report, NRL Memorandum Report 6096, March 1988.

9. Trizna, D.B., "Measurement and Interpretation of North Atlantic Ocean Marine Radar Sea Scatter," NRL Report 9099, April, 1988.

END
DATED
FILM
8—88
DTIC